Cell PRESS
Neuron
Article

Voltage-Sensing Domain of Voltage-Gated Proton Channel Hv1 Shares Mechanism of Block with Pore Domains

Liang Hong,[1] Medha M. Pathak,[1] Iris H. Kim,[1] Dennis Ta,[1] and Francesco Tombola[1,*]
[1]Department of Physiology and Biophysics, University of California, Irvine, CA 92697, USA
*Correspondence: ftombola@uci.edu
http://dx.doi.org/10.1016/j.neuron.2012.11.013

SUMMARY

Voltage-gated sodium, potassium, and calcium channels are made of a pore domain (PD) controlled by four voltage-sensing domains (VSDs). The PD contains the ion permeation pathway and the activation gate located on the intracellular side of the membrane. A large number of small molecules are known to inhibit the PD by acting as open channel blockers. The voltage-gated proton channel Hv1 is made of two VSDs and lacks the PD. The location of the activation gate in the VSD is unknown and open channel blockers for VSDs have not yet been identified. Here, we describe a class of small molecules which act as open channel blockers on the Hv1 VSD and find that a highly conserved phenylalanine in the charge transfer center of the VSD plays a key role in blocker binding. We then use one of the blockers to show that Hv1 contains two intracellular and allosterically coupled gates.

INTRODUCTION

The Hv1 voltage-gated proton channel (also known as HVCN1 or VSOP) is a member of the superfamily of proteins containing voltage-sensing domains (VSDs) (Ramsey et al., 2006; Sasaki et al., 2006). These domains are made of four membrane-spanning segments (S1 through S4), and their function is to detect changes in membrane potential in both excitable and nonexcitable cells (Figure 1A) (Okamura, 2007; Yu and Catterall, 2004). Voltage-gated sodium, potassium, and calcium channels are also VSD-containing proteins. They are all made of a pore domain (PD) responsible for selective ion permeation, and four VSDs. A gate located on the intracellular side of the PD (known as activation gate) opens and closes as a function of membrane potential due to direct interaction with the VSDs (Hille, 2001) (Figure 1B).

The Hv1 channel does not have a pore domain and its VSD is responsible for proton permeation (Lee et al., 2009; Ramsey et al., 2006; Sasaki et al., 2006). The S4 segment, which contains voltage-sensitive arginines highly conserved in other voltage-gated ion channels, is directly connected to a C-terminal coiled-coil domain (Figure 1A). Hv1 has been shown to form dimers in which two VSD subunits are held together by the coiled-coil domain (Figures 1A and 1B) (Koch et al., 2008; Lee et al., 2008; Li et al., 2010; Tombola et al., 2008). The deletion of the Hv1 N and C-terminal domains, as well as the substitution of these domains with the corresponding parts of the voltage-sensitive phosphatase Ci-VSP (Murata et al., 2005), were found to produce monomeric channels capable of voltage-dependent proton conduction, indicating that the gating machinery is contained in each VSD (Koch et al., 2008; Tombola et al., 2008). The nature of this gating machinery and the location of the activation gate in the VSD are still unknown.

Open channel blockers are inhibitors that bind the ion permeation pathway of a channel only when its gate is open (Hille, 2001). We reasoned that if open channel blockers were available for ion permeable VSDs, they could be used to study the gating mechanism of Hv1 and, in particular, to locate the activation gate in the VSD. Here, we describe guanidine derivatives that bind the Hv1 channel from the intracellular side of the membrane and act as potential channel blockers. We find that the most effective of these compounds, 2-gunaidiniumbenzimidazole (2GBI), can access the core of the VSD only when the channel is in the open conformation and that the highly conserved phenylalanine 150 in the S2 transmembrane helix plays a key role in blocker binding. We then use mutations at position 150 to characterize the interaction between the blocker and the VSD gating machinery.

As previously shown for the pore domain, we find that the activation gate of the VSD is located on the intracellular side of the membrane and that when 2GBI is bound to its receptor the gate cannot close ("foot in the door" mechanism of block). By comparing the recovery from block of dimeric and monomeric Hv1 channels, we find that once one of the two subunits releases its blocker, the state of its gate determines the rate of blocker unbinding from the neighboring subunit. We discuss the structural implications of this mechanism of block for the VSD's intracellular vestibule, and for the coupling between the gates in the channel's two subunits.

The Hv1 channel is known to play important roles in proton extrusion, pH homeostasis, and production of reactive oxygen species in a variety of cell types (Capasso et al., 2011). It has been recently implicated in cancer development (Wang et al., 2012) and brain damage during ischemic stroke (Wu et al.,

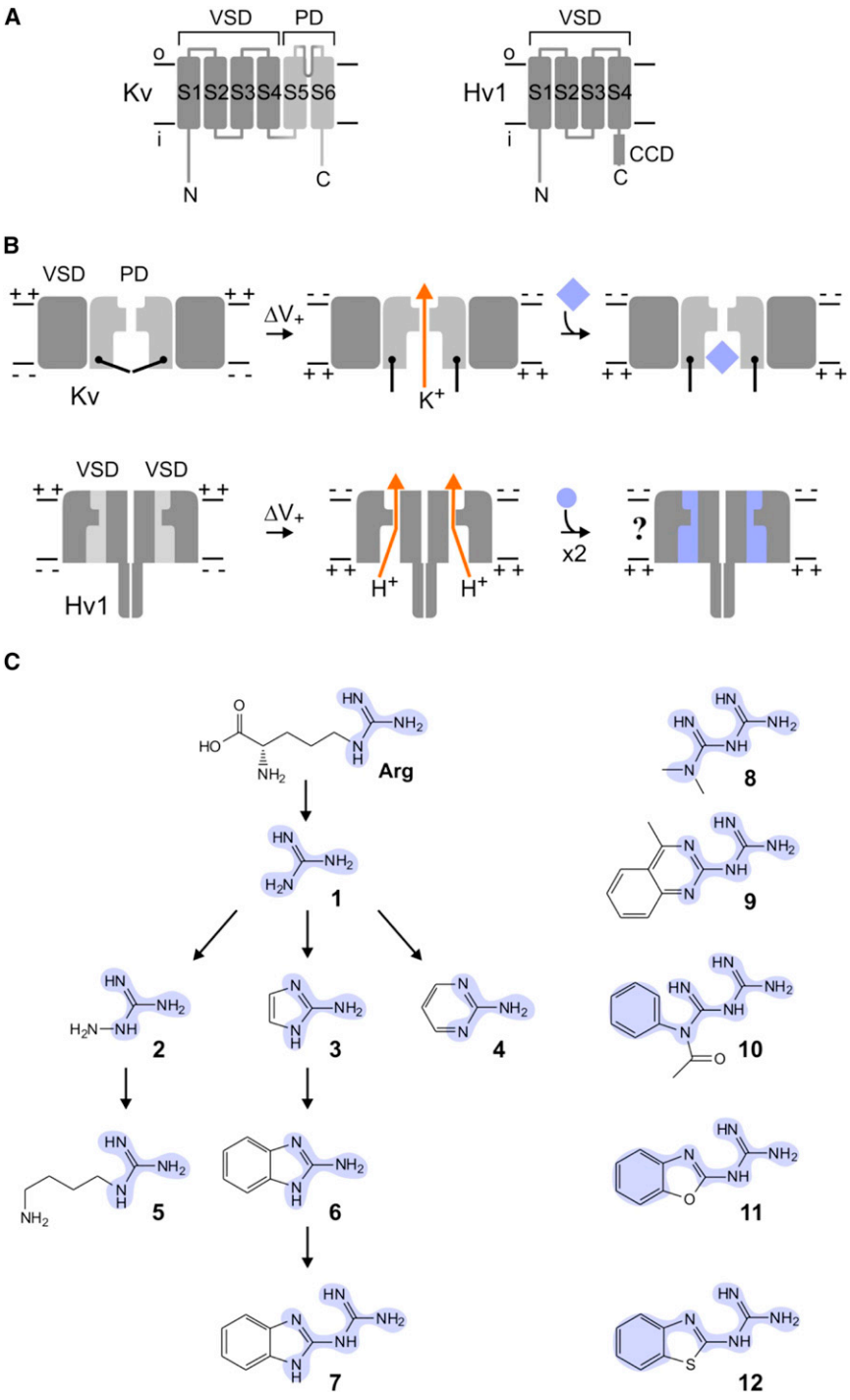

Figure 1. Gating of a VSD Pore Probed with Intracellular Blockers

(A) Topology of VSD-containing channels with and without a pore domain (PD). CCD: coiled-coil domain.

(B) Voltage-dependent opening and block of PD (top) and VSD (bottom). The Hv1 channel contains two conducting VSDs. The location of its activation gates is not known, nor is the mechanism of VSD block. Only two of the four Kv VSDs are shown for clarity.

(C) Guanidine derivatives tested as potential Hv1 intracellular blockers. [1] Guanidine, [2] aminoguanidine, [3] 2-aminoimidazole, [4] 2-aminopyrimidine, [5] agmatine, [6] 2-aminobenzimidazole, [7] 2-guanidinobenzimidazole, [8] metformin, [9] 2-guanidino-4-methylquinazoline, [10] N-(guanidino-imino-methyl)-N-phenylacetamide, [11] 1-(1,3-benzoxazol-2-yl)guanidine, [12] 1-(1,3-benzothiazol-2-yl)guanidine. Guanidine moieties are highlighted in blue in compounds 1–7. The parts of compound 7 that are conserved in compounds 8–12 are also highlighted in blue.

RESULTS

Inhibition of Hv1 Channels by the Guanidine Derivative 2GBI

Guanidinium was previously found to permeate the VSDs of mutated voltage-gated sodium and potassium channels (Sokolov et al., 2010; Tombola et al., 2005), and to inhibit Hv1 without shifting the channel's activation curve (Tombola et al., 2008). Because of its structural similarity to the S4 voltage-sensing arginines, guanidinium appeared to be a good starting compound to develop inhibitors that bind to the core of the VSD. Guanidinium is effective at inhibiting proton currents in the millimolar concentration range. We hypothesized that more complex molecules containing the guanidine moiety could have a higher binding affinity for Hv1. We screened guanidine derivatives with different steric features (Figure 1C) on inside-out patches from *Xenopus* oocytes expressing the human Hv1 channel. The proton current elicited by depolarization to +120 mV was measured before and after addition of each compound to the bath solution at the final concentration of 200 μM (Figures 2A–2C). Compounds 3, 5, 6, 7, 9, and 12 were found to be more effective at inhibiting Hv1 than guanidinium (compound 1), while the other compounds were equally or less effective than guanidinium. The inhibition was fully reversible for all the compounds. With the exception of compound 4, the protonated and positively charged forms of the tested inhibitors are expected to be the most abundant in

2012). Understanding how compounds like guanidine derivatives interact with the channel's VSD and block proton conduction is an important step toward the development of pharmacological treatments for diseases caused by Hv1 hyperactivity. In addition, it can provide important clues on how to block VSDs of other voltage-gated ion channels when they become ion permeable as a result of naturally occurring mutations (Sokolov et al., 2007).

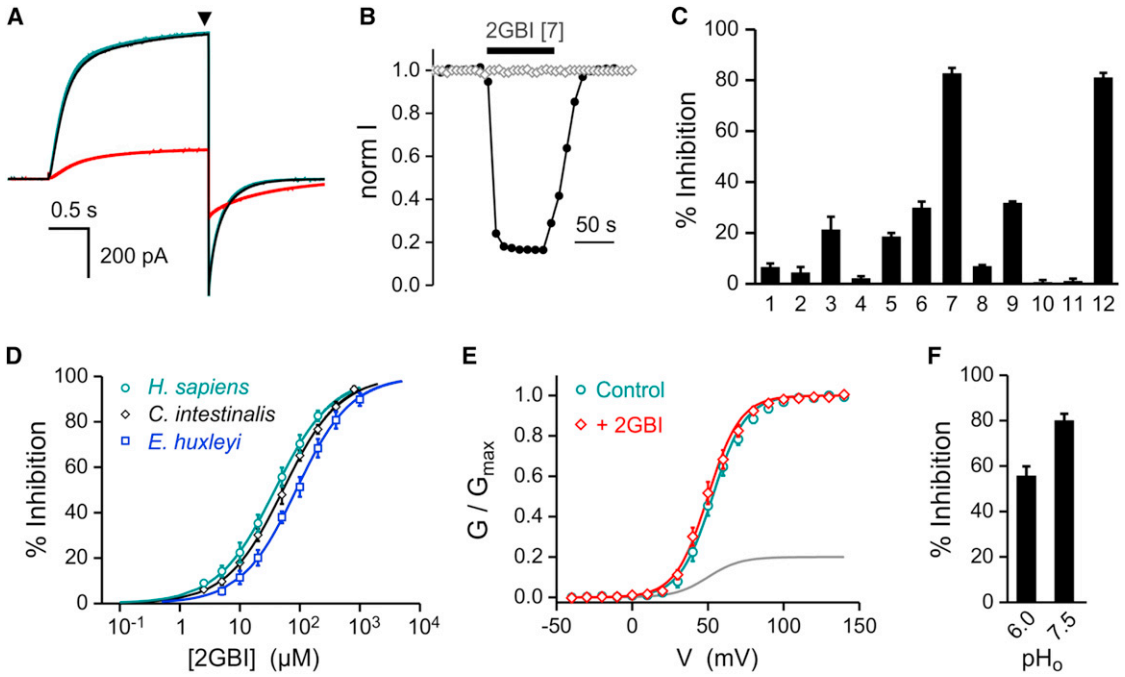

Figure 2. Inhibition of Proton Channel Activity by Guanidine Derivatives

(A) Proton currents measured in an inside-out patch from a *Xenopus* oocyte expressing WT human Hv1 before (black trace) and after (red trace) addition 2GBI (compound #7) in the bath solution (200 μM). Teal trace (overlapping black trace) is the current measured after inhibitor washout. Currents were activated by depolarizations to +120 mV from a holding potential of −80 mV. $pH_i = pH_o = 6.0$. The current measured at the end of the depolarization step (black triangle) was used to produce plots like the one shown in (B).

(B) Time courses of inhibition produced by 200 μM intracellular 2GBI (black circles), or by 500 μM extracellular 2GBI (gray diamonds). Solid bars indicate the presence of the inhibitor in the bath during measurements performed in inside-out (black), or outside-out (gray) patch configuration.

(C) Average inhibition produced by the indicated compounds (numbers as in Figure 1) added intracellularly (200 μM).

(D) Dose dependence of 2GBI inhibition for proton channels of the indicated species. Curves are Hill fits of the data points (see Table S1).

(E) G-V relationships for human Hv1 in the presence and absence of 200 μM 2GBI ($pH_i = pH_o = 6.0$.). Teal and red curves are Boltzmann fits (see Table S2). Gray line is the G-V in the presence of the inhibitor normalized to the control maximal conductance (no inhibitor).

(F) Effect of extracellular pH on proton channel inhibition by 50 μM intracellular 2GBI ($pH_i = 6.0$). Error bars are ± SEM, $n \geq 4$.

See also Figures S1 and S2.

solution at the pH used for the measurements (see Figure S1 available online).

We first examined compounds 1 through 7 and found that when the guanidine structure was part of a five-membered aromatic ring, the resulting inhibitors blocked the proton current more effectively than guanidinium alone (e.g., compounds 3 and 6 in Figures 1C and 2C). The presence of a second guanidine group, conjugated with the one on the ring, in compound 7 (2GBI) further increased the affinity for the channel (Figures 1C and 2A–2D). We then examined compounds 8 through 12 to gain insight on the molecular features that make 2GBI the most effective inhibitor. Compounds 8, 9, and 10 share with 2GBI the conjugated double guanidine substructure but were not as effective as 2GBI at inhibiting the proton channel. Compounds 11 and 12 differ from 2GBI and from each other only at one position in the five-membered ring. However, compound 12 inhibited the proton current almost as effectively as 2GBI while compound 11 was even less effective than simple guanidinium. These results indicate that the binding site for guanidine derivatives on the proton channel is highly selective.

Transient application of 2GBI on the intracellular side of the membrane while the channels were held open at +120 mV resulted in fast current reduction (Figure S2A). Transient application of the compound before the channels were opened had no effect on the current elicited by subsequent depolarization (Figure S2A). When 2GBI was applied before the depolarization step and maintained throughout the recording, the current reached a steady-state level of inhibition with the same kinetics of channel opening. The same steady-state level was reached more rapidly when the inhibitor was applied during the depolarization step (Figure S2B).

2GBI failed to inhibit the outward Hv1 current elicited by depolarization at +120 mV and the inward tail current generated during membrane repolarization at −80 mV when added to the bath solution in outside-out patch configuration (Figures 2B, S2C, and S2D). The strong sensitivity of Hv1 to intracellular 2GBI and the lack of sensitivity to extracellular 2GBI (measured over the same timescale and concentration range) imply that the binding site on the channel is directly accessible only from the intracellular side of the membrane. However, slow

membrane crossing by guanidine derivatives has been previously observed (Kalia and Swartz, 2011). So, we cannot exclude that longer treatments with extracellular 2GBI than the ones tested here could result in Hv1 inhibition.

To determine whether the binding site for 2GBI is located in a structurally conserved part of the protein, we compared the dose dependence of inhibition of the human channel to the dose dependences of inhibition of Ci-VSOP, the channel from the tunicate *Ciona intestinalis* (Sasaki et al., 2006), and Eh-HVCN1, the channel from the coccolithophore *Emiliana huxleyi* (Taylor et al., 2011) (Figure 2D; Table S1). Ci-VSOP and Eh-HVCN1 conduct protons through their VSDs like the human Hv1, and they are 27% and 18% identical to the human protein, respectively. Despite some differences in IC_{50} (38 μM for the human Hv1, 52 μM for Ci-VSOP, and 87 μM for Eh-HVCN1), 2GBI was able to completely inhibit the three channels within similar concentration ranges indicating that the binding site has been maintained over evolution. Given the higher sensitivity of the human Hv1 for 2GBI, we continued our study of the mechanism of inhibition with this channel.

2GBI Interaction with the Open VSD

We then asked whether 2GBI acts as an allosteric modulator like other known Hv1 inhibitors (Alabi et al., 2007; DeCoursey and Cherny, 2007), or as a channel blocker. If 2GBI inhibits the Hv1 current by making channel opening more difficult, its binding should alter the channel's voltage dependence of activation. We verified this by comparing the G-V curves of Hv1 in the presence of 200 μM 2GBI and in the absence of the inhibitor. The curves were obtained from tail current measurements as previously described (Musset et al., 2008; Tombola et al., 2010) and were found to be superimposable (Figure 2E; Table S2). The finding that 2GBI reduces the channel's maximal conductance without altering its G-V curve and the observation that channels already opened by depolarization can be quickly inhibited by fast application of 2GBI (Figures S2A and S2B) are consistent with a mechanism of inhibition in which 2GBI blocks open channels. We also found that the efficiency of Hv1 block by intracellular 2GBI increased when the concentration of protons on the extracellular side of the membrane decreased (higher pH_o) (Figure 2F), suggesting that the blocker binds in the channel's pore where it can interact with permeating protons. To gain more insight on whether 2GBI has access to the proton permeation pathway inside the VSD, we analyzed the effects of the transmembrane electric field and extracellular protons on 2GBI inhibition.

Because of its positive charge, 2GBI is expected to be sensitive to the transmembrane electric field when binding to the channel. This means that its apparent dissociation constant (K_D) should depend on the membrane potential. We determined the voltage dependence of K_D by measuring the proton current carried by maximally open channels in the presence of 50 μM 2GBI at different membrane potentials (Figures 3A and 3B), and by using as reference the K_D measured from the dose-response curve of Figure 2D at +120 mV (see Supplemental Experimental Procedures, Equations S4 and S5). From the exponential fit of the K_D-voltage relationship the parameter δz_b (effective charge) of 0.35 ± 0.1 was calculated (see Supplemental Experimental Procedures, Equation S6), which provides an estimate of the maximal fraction of the transmembrane electric field that the blocker must cross in order to reach its binding site inside the channel (Woodhull, 1973). Considering a relative drop in membrane potential from 1 to 0 across the entire Hv1 proton permeation pathway, a δz_b of 0.35 means that the charged 2GBI molecule (z_b = +1) experiences up to 35% of the total electric field when moving in and out of the proton pore.

If 2GBI binds the VSD on the intracellular side of the permeation pathway, protons entering the channel from the extracellular side are expected to facilitate blocker unbinding. Accordingly, an increase in extracellular proton concentration (decrease in pH_o) is expected to cause an increase in the rate of blocker unbinding at negative potentials, resulting in a faster decay of the tail current. To test the effect of extracellular protons on blocker unbinding, we compared the decays of the tail current at −40 mV measured at two different extracellular pHs (Figure 3C). We first determined the pH_o dependence of channel closing by measuring the ratio between the time constants of current decays at pH_o 7.5 and 6.0 in the absence of the blocker ($\tau_{7.5}/\tau_{6.0}$ ~1.5). Then, we determined the pH_o dependence of channel unblocking by similar measurements carried out in the presence of 200 μM 2GBI in the intracellular solution (see Supplemental Experimental Procedures). As expected, we found that increasing the extracellular proton concentration significantly shortens the decay time of the tail current in the presence of the blocker ($\tau_{7.5}/\tau_{6.0}$ ~2.6) (Figure 3D). This is consistent with blocker unbinding facilitated by extracellular protons in the permeation pathway.

F150 Plays a Key Role in 2GBI Binding

Since 2GBI appears to bind the Hv1 channel somewhere along the permeation pathway, we planned to use it to shed light on the location of the pore. We wondered whether we could find residues in the channel that, when mutated, would strongly affect 2GBI binding. We had previously identified a mutant of the Shaker potassium channel that conducts ions—including guanidinium—through its VSD (Tombola et al., 2005) and had found several residues that are likely to line the Shaker VSD pore (Tombola et al., 2007). We hypothesized that among the Hv1 residues homologous to those involved in ion permeation in the Shaker VSD there could be some that face the proton pore and participate in the binding of 2GBI. Of all the Shaker mutations tested for their impact on the ion current (omega current) flowing through the VSD, those at position F290 produced the strongest effect (Tombola et al., 2007). In addition, F290 was proposed to be part of the occlusion (charge transfer center) that prevents ions from flowing through nonconducting VSDs (Tao et al., 2010). The Hv1 residue F150 corresponds to the Shaker F290. The phenylalanine is located deep within the membrane in the S2 helix, and it is highly conserved in the VSDs of voltage-gated ion channels and voltage dependent phosphatases. We mutated F150 to several other residues and found that the alanine substitution produced a ~360-fold increase in binding affinity for 2GBI (Figure 4 and Table S1). The cysteine substitution also increased the affinity for the blocker, but to a lesser extent (Figure 4C). On the other hand, the dose dependence of block of Hv1 F150W was very similar to the wild-type (WT) channel (Figure 4C). These findings show

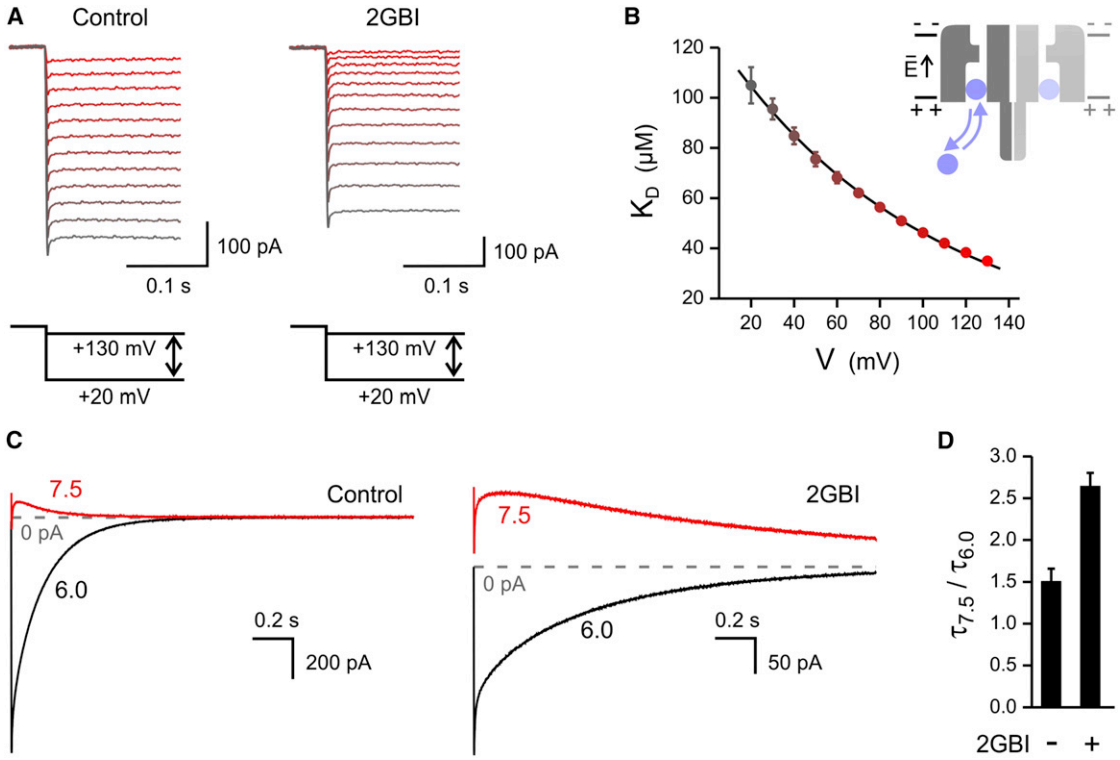

Figure 3. 2GBI Binding and Unbinding Depend on Membrane Potential and Extracellular Proton Concentration

(A) Proton currents from Hv1 channels measured in inside-out patches in the absence of blocker (Control) and in the presence of 50 μM 2GBI in the bath solution ($pH_i = pH_o = 6.0$). Patches with similar current levels were selected for the comparison and scaled to match the maximal current. A depolarization to +140 mV was followed by a step to a progressively lower voltage, in 10 mV decrements. Holding potential was −80 mV. The color of the traces transitions from gray to red as the test voltage becomes more positive.

(B) Apparent dissociation constant of 2GBI block as a function of membrane potential, calculated from proton currents recorded using the voltage protocol described in (A). Error bars are ± SEM, n = 6. The exponential fit of the data is shown as black line.

(C) Hv1 tail-currents measured from two outside-out patches in response to a voltage step to −40 mV from a preceding depolarization at +120 mV (not shown). pH_i was 6.0. For each patch, currents were measured at a pH_o of 6.0 and 7.5. Traces on the right were measured in the presence of 200 μM 2GBI in the intracellular (pipette) solution.

(D) Average values of the ratio of time constants of current decay measured at pH_o = 7.5 and 6.0, from traces like those reported in (C). Time constants were calculated from multiexponential fits of current decays. A $\tau_{7.5}/\tau_{6.0} > 1$ means that the decay is faster when the proton concentration is higher on the extracellular side of the pore.

Error bars are SEM, n ≥ 4.

that the nature of the side chain at position 150 strongly affects the strength of the interaction between the channel and 2GBI.

In Shaker, mutations at position F290 were found to alter the voltage dependence of gating, producing shifts in the conductance versus voltage relationship (G-V curve), and alterations of the gating charge movement in the VSD (Lacroix and Bezanilla, 2011; Tao et al., 2010). We determined the G-V curves of Hv1 F150A, F150C, and F150W and compared them to the G-V of the WT channel (Figure 4B; Table S2). We found that mutation F150W produced the strongest perturbation of channel gating (largest G-V shift compared to WT), and yet it had almost no effect on 2GBI binding. In contrast, mutations F150A and F150C produced different effects on 2GBI binding, but the same effect on channel gating (very similar G-V curves). We conclude that there is no correlation between the alterations of channel gating and affinity for the blocker produced by F150 substitutions. This suggests that the mechanism by which F150 mutations alter 2GBI binding is distinct from the mechanism by which they alter the movement of the voltage sensor.

Selectivity of the Perturbations of F150 Substitutions

We examined whether the increase in affinity for 2GBI resulting from mutations at position 150 was dependent on the structure of the inhibitor. We compared the relative block of F150A and WT channels by 2GBI to the relative block of the same two channels by other two intracellular inhibitors: guanidinium and magnesium. Guanidinium was selected for the comparison because it lacks the 2GBI structural feature provided by the benzimidazole group. Magnesium was selected because it was found to inhibit the Hv1 proton current despite being structurally unrelated to 2GBI and guanidinium. We found that, while there is a large difference in binding affinity for 2GBI between F150A and WT channels, there is a much smaller difference for guanidinium and no difference for magnesium (Figure 4D).

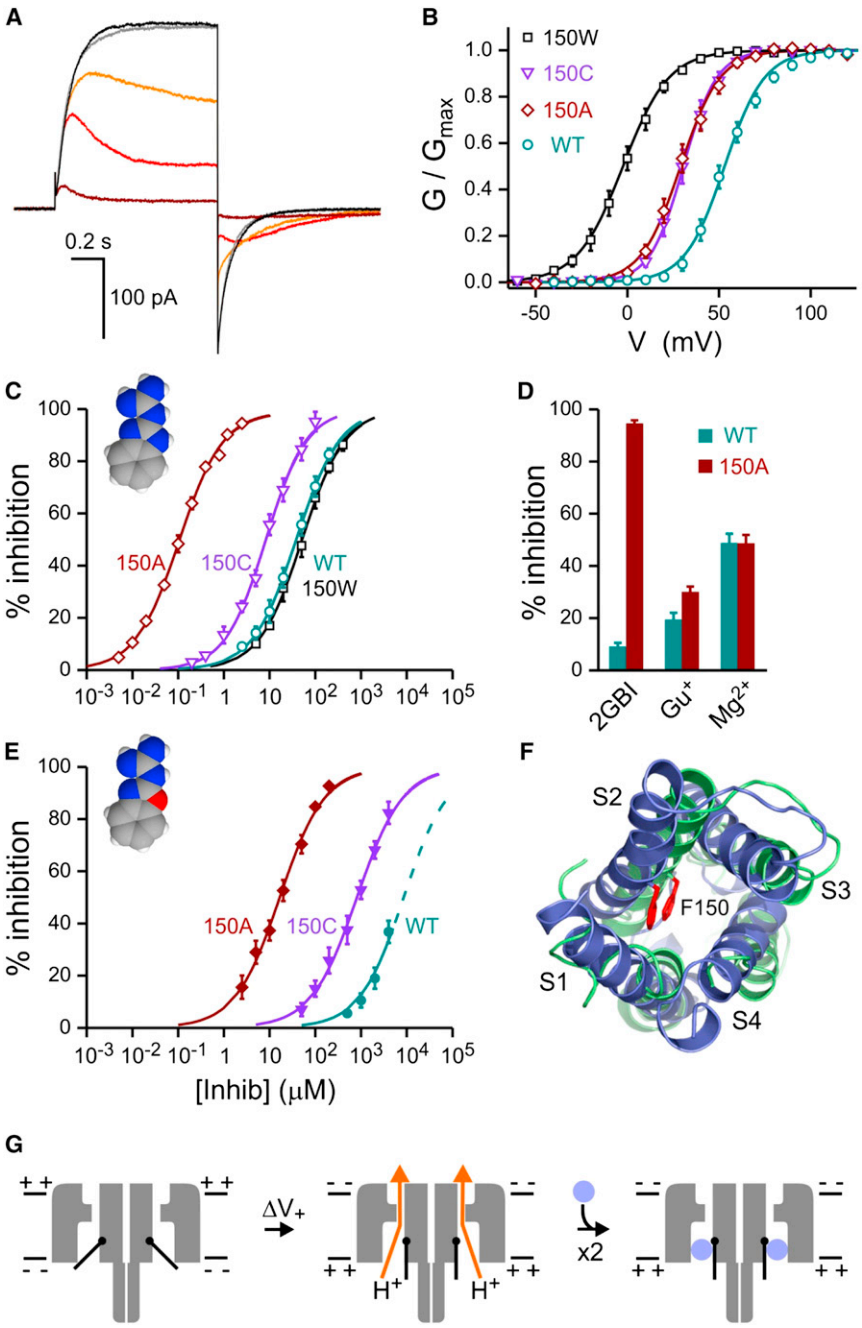

Figure 4. Effects of F150 Substitutions on Hv1 Voltage Dependence and Inhibition by Intracellular Blockers

(A) Proton currents measured from F150A Hv1 channels in response to depolarizations to +120 mV from a holding potential of −80 mV ($pH_i = pH_o = 6.0$.). After recording the current from an inside-out patch in the absence of the inhibitor (black trace), 2GBI (2 μM) was added to the bath solution (dark red trace) and then removed by bath perfusion (gray trace). Red and orange traces show partial recovery from block during inhibitor washout.

(B) Conductance versus voltage relationships for the indicated F150 mutants compared to WT (see Table S2).

(C) Dose dependence of 2GBI inhibition of F150A, F150C, and F150W channels compared to WT. Curves are Hill fits (see Table S1).

(D) Inhibition of Hv1 F150A and WT by 1 μM 2GBI, compared to inhibition by guanidinium (500 μM) and magnesium (7.9 mM).

(E) Dose dependence of inhibition by 2GBOZ (compound #11) of F150A and F150C channels compared to WT. Curves are Hill fits (see Table S1). Extrapolation of the WT inhibition curve at concentrations higher than the solubility limit of 2GBOZ is shown as dashed line. Error bars are ± SEM, $n \geq 4$ (not shown when smaller than symbols).

(F) Location of phenylalanine 150 (red side chain) in the two structural models of the Hv1 VSD from Wood et al. (2012) (R1-model in green, and R2-model in blue). The models were superimposed by distance minimization of the alpha carbons of the S1 segments (residue 99–123). The VSD is shown from the intracellular side of the membrane plane.

(G) Interpretation of the result shown in (A) as state dependent block regulated by the opening of an activation gate.

We also examined the inhibition of F150A, F150C, and WT channels by 1-(1,3-benzoxazol-2-yl)guanidine (GBOZ) (compound 11 in Figure 1). This inhibitor is very similar to 2GBI in structure, but it is a weak blocker like magnesium (both GBOZ and magnesium have IC_{50}s close to 9 mM). We found that the F150A and F150C mutations altered the affinity of the channel for GBOZ in the same way that they altered the affinity for 2GBI (Figure 4E). This shows that the nature of the side chain of residue 150 affects the interaction between the channel and the inhibitor in a selective manner, with 2GBI and closely related compounds being affected the most.

Opening of an Intracellular Gate Is Required for 2GBI Binding

When Hv1 WT is treated with 2GBI, the proton current is inhibited, and the apparent rate of channel deactivation is slowed down, producing a more persistent inward current at negative voltages after depolarization (Figures 2A and S2C). A similar phenomenon is observed with other voltage-gated ion channels when their pore domain interacts with intracellular blockers. When the intracellular activation gate of the pore domain is closed, blockers are prevented from reaching a binding site located in the core of the permeation pathway. If the channel opens and the blocker is allowed to bind, the gate cannot close until the blocker unbinds. This is referred to as foot in the door effect (Yeh and Armstrong, 1978), and it is also seen with the inactivation ball of some fast inactivating channels (Hille, 2001). The apparent rate of channel deactivation is slowed down by the foot in the door effect because the gate cannot close right away upon membrane repolarization and must

instead wait for the blocker (or the inactivation ball) to first vacate the pore.

The foot in the door effect of 2GBI on the Hv1 deactivation rate suggests that there is an intracellular gate in the VSD also. However, when channels with intracellular gates are opened in the presence of a blocker, the time course of current activation usually displays a biphasic behavior. Upon depolarization, the current first raises, reaches a maximum, and then falls to a steady-state level that depends on the affinity and concentration of the blocker. This is observed, for example, when voltage-gated potassium channels are blocked by intracellular quaternary-ammonium inhibitors (Armstrong, 1968, 1971; Choi et al., 1993), or by the inactivation ball (Armstrong and Bezanilla, 1977; Demo and Yellen, 1991; Zagotta et al., 1990). The biphasic behavior is a direct result of gate opening. At the beginning of the depolarization, most channels are closed and cannot bind the blocker. Open channels are generated faster than they are blocked and the current increases. Over time, as the pool of closed channels decreases, the production of open channels slows down and the blocking process becomes dominant, with consequent decrease in the current.

When 2GBI inhibits Hv1 WT, there is no sign of a biphasic behavior in the activation current (Figure 2A). The proton current increases upon depolarization with similar kinetics in the presence and in the absence of the blocker. However, when 2GBI inhibits Hv1 F150A, it produces a strong change in the kinetics of the activation current, which becomes clearly biphasic (Figure 4A). This, in combination with the prominent slowdown of the deactivation current, provides strong evidence for the regulation of 2GBI block by an intracellular gate (Figure 4G).

The behavior of Hv1 F150A also helps explain why 2GBI does not affect the kinetics of activation in the WT channel. The slow-opening process in Hv1 WT does not allow a transient accumulation of open channels in the presence of 2GBI. The channels simply get blocked as soon as they open, making it impossible for the current to display the biphasic time course. The F150A mutation changes all this, directly, by speeding up the opening process (compare time scales in Figures 2A and 4A), and indirectly, by lowering the concentration of 2GBI required for inhibition (increased affinity), which results in a slower rate of channel block.

Coupling between Gates in the Two Hv1 Subunits

To further investigate the interaction between 2GBI and the Hv1 intracellular gate, we examined the recovery from block of the F150A mutant with a two-pulse voltage protocol (Figure 5A). The current measurements were performed in inside-out patches and in the presence of 400 nM blocker in the bath solution. The channels were opened and blocked with the first depolarization pulse. They were then unblocked by applying a negative voltage, and the fraction of recovery from block was tested with a second depolarization pulse. The time between the two pulses (t_{IP}) spent at negative voltage was varied to capture the time course of recovery (Figures 5A–5C). This was determined by reporting the relative increase in peak current at the test pulse as a function of t_{IP}.

When t_{IP} is short, only a few channels have the time to recover from block before the second depolarization. This is expected to result in a peak current in the second pulse similar in magnitude to the current at the end of the first pulse. When t_{IP} becomes longer, the channels have more time to recover and the peak current in the second pulse should gradually increase until there is no more difference between the first and second peaks (complete recovery). This is the typical behavior of current recovery from block/inactivation observed in voltage-gated channels with pore domains. But, Hv1 F150A recovers from 2GBI block in a significantly different way. As t_{IP} increases, the second peak increases very fast and reaches a maximum value that is higher than the first peak. Then, at longer t_{IP}, the second peak slowly decays to reach the value of the first peak (Figures 5A and 5C). In addition, the recovery peak currents measured at short and long t_{IP} display very different kinetics of opening and block (compare peaks 1 and 2 in Figure 5D, and values of τ_{decay} in Figure 5E). If the recovery peaks were produced only by the opening of nonblocked channels, they should only change in size as a function of t_{IP}, but their kinetics should stay the same. The difference in kinetics indicates that different populations of channels are responsible for the recovery peaks at short t_{IP} versus long t_{IP}. The significant delay between the time at which the recovery peaks reach their maximum and the time at which the tail current is maximal (Figures 5A and S5A) suggests that a significant fraction of the recovery current comes from a population of channels that are not able to conduct current at negative potentials but can become conductive very rapidly at positive potentials.

While voltage-gated sodium, potassium, and calcium channels contain one activation gate in the pore domain, Hv1 is made of two subunits that can gate cooperatively (Fujiwara et al., 2012; Gonzalez et al., 2010; Musset et al., 2010; Tombola et al., 2010). We considered that the presence of two coupled gates in Hv1 could be the reason for its peculiar recovery from block. We first tested this hypothesis by examining the recovery from block of monomeric Hv1 F150A. Monomerization was achieved as previously described by replacing Hv1 intracellular N and C termini with the corresponding parts of Ci-VSP (Tombola et al., 2008). We found that the N_{VSP}-Hv1-C_{VSP} F150A chimera recovers from block similarly to channels with pore domains, with the current of the second peak gradually rising to the level of the first peak as t_{IP} increases (Figures 5B and 5C). Moreover, the kinetics of opening and block of the recovery peaks measured at short and long t_{IP}s were the same in monomeric channels (Figures 5D and 5E).

Models of Channel Block in Dimeric and Monomeric Hv1

We examined the recovery from block by simulating the gating process in the presence of 2GBI with kinetic schemes involving one gate (monomer) (Figure S3), or two coupled gates (dimer) (Figure 6). We assumed that each subunit can exist in three different states: closed (C), open (O), or blocked (B). This produces a total of nine states in dimeric channels: CC, OC (equivalent to CO), OO, BO (equivalent to OB), BC (equivalent to CB), and BB (Figure 6A). Since we found that 2GBI must wait for the activation gate to open in order to block the channel, we assumed that the blocked state can only be reached from the open state in each individual subunit.

We had previously established that the opening of one Hv1 subunit strongly facilitates the opening of the other subunit

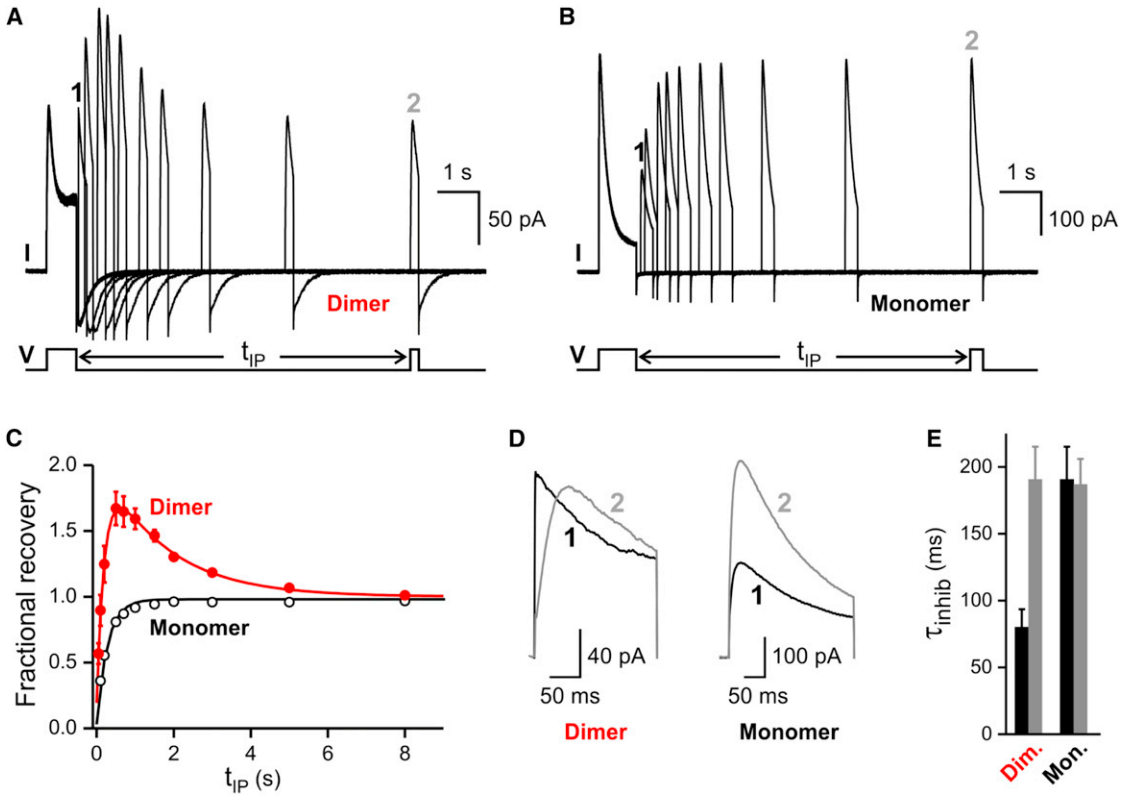

Figure 5. Recovery from Block of Hv1 F150A: Dimer versus Monomer

(A) Proton currents from F150A Hv1 channels in the presence of 400 nM 2GBI measured in response to the indicated two-pulse voltage protocol. The time interval between depolarization pulses (t_{IP}) was progressively increased from 0.05 to 8 s. The trace recorded with the shortest t_{IP} is not displayed for clarity. The voltage was stepped from −60 mV to +140 mV in both pulses. Holding potential between sweeps was −80 mV.

(B) Proton currents from monomeric F150A N_{VSP}-Hv1-C_{VSP} chimera, measured under the same conditions as in (A).

(C) Fractional recovery from block as a function of t_{IP} calculated from peak currents measured as shown in (A) and (B). Red filled circles are for F150A Hv1. Black open circles are for the F150A N_{VSP}-Hv1-C_{VSP} chimera. Red line is a double-exponential fit of the data points for the dimer. Black line is a monoexponential fit of the data points for the monomer.

(D) The first and last recovery peaks marked as 1 and 2 in (A) and (B) (t_{IP} = 0.2 s and 8 s, respectively) are compared. The peaks are superimposed and magnified to show their kinetics.

(E) Apparent time constants of 2GBI block during the second pulse of two-pulse protocols. The constants were measured by monoexponential fit of the decaying current in recovery peaks 1 (black columns) and 2 (gray columns). Error bars are ± SEM, n ≥ 4.

See also Figure S3.

(Tombola et al., 2010). We found that the inclusion of facilitated opening in the kinetic model of dimeric Hv1 was required to reproduce the observed time course of recovery from block. This was accomplished by making opening transitions from states with one gate already open (e.g., OC → OO, and BC → BO) faster than equivalent transitions from states with both gates closed (e.g., CC → OC). In order to reproduce the experimental findings, the model needed to include also the following properties of channel block: (1) when the blocker is bound to one subunit, the gate of that subunit cannot close (foot in the door), and (2) if the gate of an unblocked subunit happens to close while the neighboring subunit is still bound to the blocker, it becomes significantly harder for that blocker to unbind. The first property was represented in the model by excluding transitions of the type BX → CX (with X = C, O, or B). The second property was represented by a slower rate of unblocking in dimers with one closed subunit (e.g., BC → OC) compared to the rate of unblocking in dimers with two open or blocked subunits (e.g., BO → OO, BB → OB).

We found that the kinetic model shown in Figures 6A and S4 can reproduce the major features of channel block and recovery from block of dimeric F150A Hv1. It can also be simplified to reproduce the observed behavior of monomeric channels (Figures S3 and S4). The simplified model features only three states (C, O, and B), loses the properties connected to the cooperative gating between subunits, but maintains the general feature of the foot in the door mechanism of block.

Using the kinetic model for the F150A dimeric channel, we were also able to reproduce the behavior of 2GBI block in the WT channel (Figure 6D). Hv1 WT is characterized by a slower rate of opening and a lower affinity for 2GBI compared to the F150A mutant. To account for these differences, adjustments in the rates of opening and block were necessary (see Figure S4). When we reduced the rates of opening and adjusted the rates of

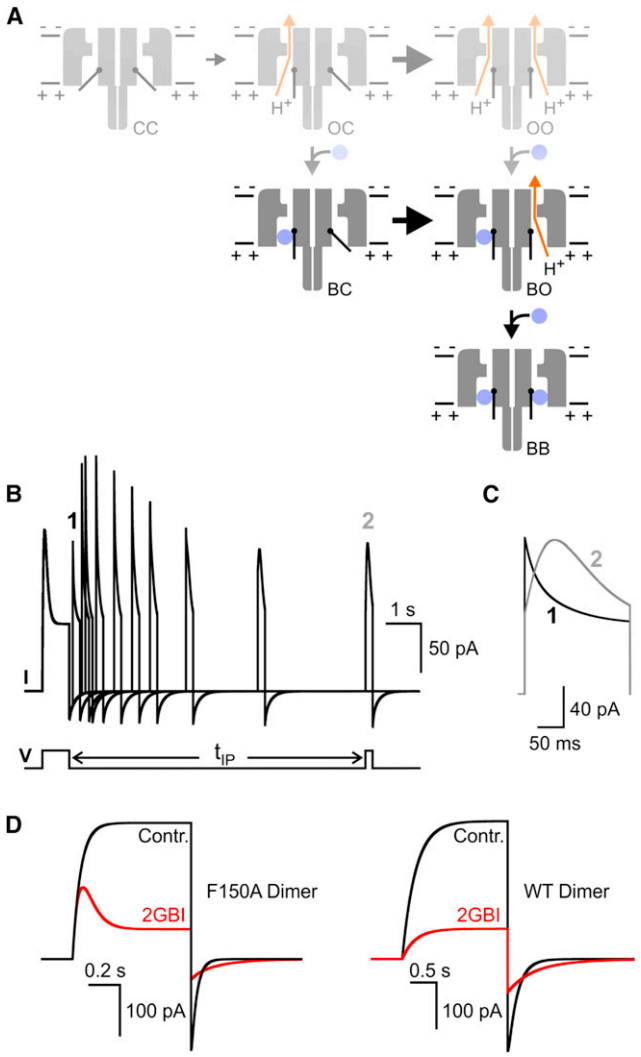

Figure 6. Model of Hv1 Opening and Block Mediated by Two Coupled Intracellular Gates

(A) States of the two gates of the Hv1 dimer during opening. CC, close-closed; OC, open-closed; BC, blocked-closed; OO, open-open; BO, blocked-open; BB, blocked-blocked. Only forward reactions favored at positive potentials are shown for clarity.

(B) Simulation of currents from modeled F150A dimeric channels generated under conditions equivalent to those reported in Figure 5A. The currents were generated using the kinetic rates reported in Figure S4.

(C) Superimposition of the first and last recovery peaks marked as 1 and 2 in (B). For analogous simulations of currents from F150A monomeric channels see Figure S3.

(D) Simulated currents from the indicated channels in response to a depolarization step to +120 mV from a holding potential of −80 mV before and after the addition of 2GBI (400 nM for Hv1 F150A and 200 μM for Hv1 WT). The currents were generated with the same kinetic model but with different rate constants to account for the slower gating, lower 2GBI binding affinity, and faster blocking and unblocking of the WT channel compared to the F150A mutant (see Figure S4).

See also Figures S4 and S5.

blocking and unblocking to account for the higher concentration of 2GBI required for block, the biphasic time course of the simulated current of F150A channels (Figure 6D, left panel) turned into the simpler time course of the WT current (Figure 6D, right panel).

State-Dependent Release of 2GBI from Dimeric Hv1

An important feature of 2GBI block highlighted by the modeling of Hv1 dimers is that, once a subunit releases its blocker, the state of its gate determines the fate of the blocker in the neighboring subunit. If the gate is open, the blocker in the other subunit is released quickly. If the gate is closed, the blocker is released slowly. We call this phenomenon "hemichannel blocker trapping" because the closing of one subunit (hemichannel formation) "traps" the blocker in the neighboring subunit. The trapping of the blocker was critically important for the simulation of the recovery from block of F150A dimers (Figure S4). We found that only models in which the BC → OC transition was much slower than the BO → OO transition (blocker trapping in BC dimers) were able to describe the experimental data. The rate of the BC → OC transition at negative potential was the parameter with the largest effect on the heights and shapes of the recovery peaks as a function of t_{IP}.

2GBI slows down the tail currents of Hv1 channels by causing a delay in gate closure. The contribution of hemichannel blocker trapping to this delay depends on the fraction of BC dimers generated. Our model indicates that the fraction of BC dimers formed at negative potentials is higher in F150A channels compared to WT channels because of the higher rate of blocker unbinding from WT subunits. Fast unblocking means that both subunits can release their blockers before the gate in either subunit can close (Figure S4). This transiently produces dimers with two open subunits and limits the formation of BC dimers in WT. The model also predicts that blockers with lower unbinding rate (higher binding affinity) than 2GBI will produce larger fractions of WT BC dimers.

The features of the interactions between 2GBI and the VSD of Hv1 are similar to those previously described for open-channel blockers of pore domains. But, the trapping of the blocker in one subunit caused by gate closing in the neighboring subunit seems to be a unique feature of Hv1, due to the existence of two distinct activation gates on two allosterically coupled ion-permeable VSDs.

Blocker Trapping Tested in Heteromeric F150A-WT Channels

We tested the conclusion that the recovery from block of Hv1 channels is delayed by 2GBI trapping in BC dimers under experimental conditions in which the formation of BC dimers is maximized. To do this, we maximized the fraction of BO dimers from which BC dimers are formed during the recovery from block at negative potentials. Generating large fractions of BO channels in WT or F150A homodimers is difficult because, even at 2GBI concentrations that produce 50% of channel block, significant fractions of dimers are in the OO and BB states at the end of the depolarization step. So, we generated linked heterodimers made of one F150A subunit and one WT subunit and exploited the large difference in 2GBI affinity between the two subunits to generate BO dimers. Based on the apparent dissociation

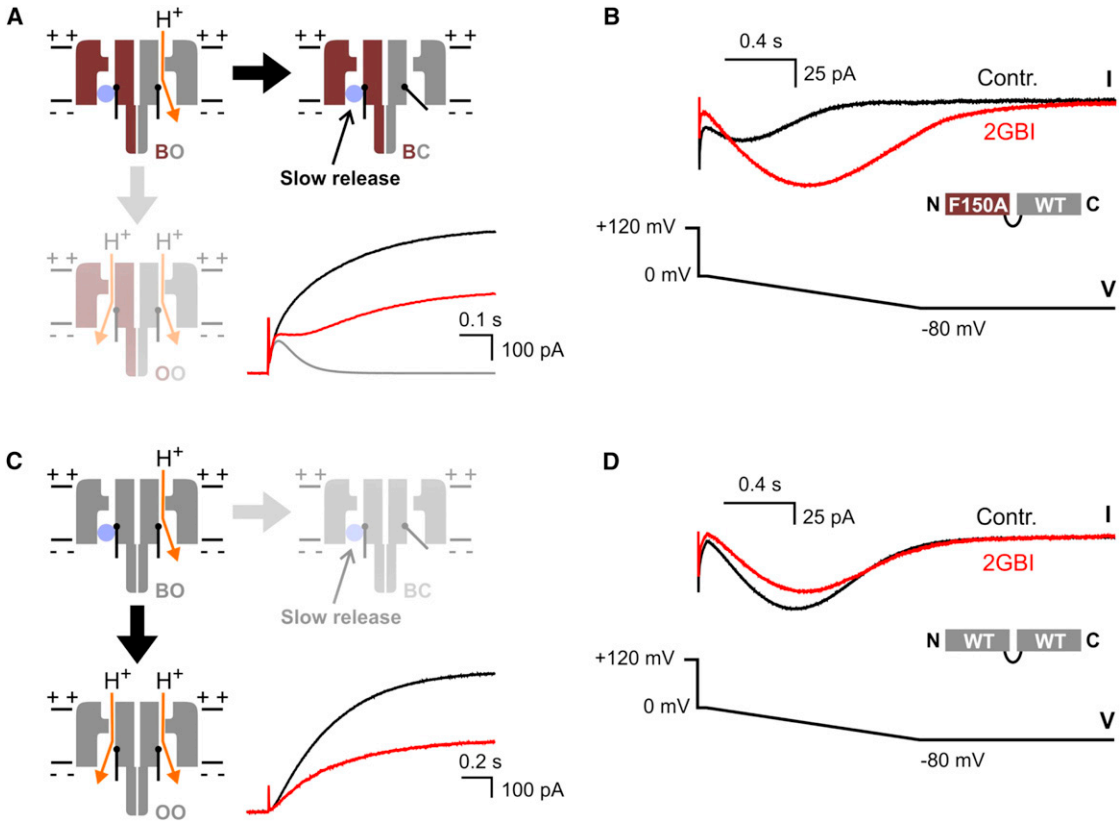

Figure 7. Hemichannel Blocker Trapping for 2GBI Tested in a Heterodimeric Hv1 Channel

(A) Partial 2GBI block of linked heterodimers made of one F150A subunit (dark red) and one WT subunit (gray). Currents traces from an inside-out patch containing F150A-WT dimers. Channels were opened by depolarization to +120 mV (from −80 mV holding potential) in the absence of the inhibitor (black trace), and in the presence of 2 μM 2GBI (red trace) in the intracellular solution ($pH_i = pH_o = 6.0$). Gray line is the predicted current contributed by the F150A subunit after 2GBI addition, obtained by multiexponential fitting of the total current measured in the presence of blocker (red trace). At the end of the depolarization, the large majority of channels are in the BO state when 2GBI is present. Upon membrane repolarization, BO channels can be converted to either BC or OO channels. Black arrow indicates favored conversion.

(B) Tail currents from linked dimers measured in response to the indicated voltage ramp after the depolarization step described in (A).

(C) Partial 2GBI block of linked WT-WT homodimers. Currents traces were measured under the conditions described in (A) but using 40 μM 2GBI. At the end of the depolarization step the channels are distributed among the BB, OO, and BO/OB states. Upon membrane repolarization the conversion from BO channels to OO channels is favored (black arrow).

(D) Tail currents from linked WT-WT dimers measured in response to the indicated voltage ramp after a depolarization step to +120 mV (same conditions described in C).

constants of 2GBI from F150A and WT homodimers, we estimated that 2 μM 2GBI should block about 94% of the F150A subunits and 6% of the WT subunits at +120 mV, producing a ~50% total inhibition of the initial current (Figure 7A). After the depolarization step to +120 mV, the membrane was repolarized with a voltage ramp from 0−80 mV, and the time course of the tail current was recorded before and after addition of 2GBI (Figure 7B).

The number of open subunits decreases over time after the end of the depolarization step due to gate closing. However, the current flowing through each individual open subunit increases during the ramp, due to the increased electrical driving force for proton movement. These two opposing factors determine the position and size of the negative peak of the tail current. We reasoned that if the blocker was trapped in BC dimers, its slow release would delay the formation of open hemichannels (OC) during the voltage ramp. These hemichannels would conduct more current than those formed at the beginning of the ramp and would cause the peak of the tail current to increase in size and to shift its position to more negative voltages. We indeed observed an increase in the tail current produced by 2GBI in the F150A-WT dimers and a right shift in the position of the peak (Figure 7B).

We then repeated the same kind of measurements in WT-WT linked dimers using a 2GBI concentration of 40 μM to inhibit 50% of the current at +120 mV (Figures 7C and 7D). We observed a small reduction in the tail current during the repolarization ramp induced by the blocker and a small shift of the peak toward more negative potentials (Figure 7D). This is in agreement with the idea that the fraction of BC dimers produced from BO dimers in WT-WT channels is reduced due to the competition of the process that converts BO dimers into OO dimers (Figure 7C).

DISCUSSION

Compounds that act as inhibitors of pore domains have been used for decades to investigate the permeation and gating mechanism of voltage-gated sodium, potassium, and calcium channels (Hille, 2001). For example, the use of open channel blockers such as quaternary ammonium ions and cationic derivatives of local anesthetics led to the discovery that the activation gate of these channels faces the inner side of the membrane (e.g., Armstrong, 1971; Holmgren et al., 1997; Narahashi et al., 1969). Here, we find that some heteroaromatic guanidine derivatives are effective inhibitors of the Hv1 proton channel and show that one of these compounds, 2GBI, acts as an open channel blocker of the VSD.

The voltage dependence of VSD block by intracellular 2GBI and the effect of extracellular protons on the rate of blocker unbinding indicate that the binding site for 2GBI is located in the channel's permeation pathway. The finding that the channel's affinity for the blocker depends on the nature of the side chain at position 150 in the core of the VSD supports this conclusion, which is also in agreement with the recent finding that nonderivatized guanidinium ions can permeate the Hv1 channel when one of its S4 arginines (R211) is mutated to a different amino acid (Berger and Isacoff, 2011). From the analysis of channel block in Hv1 WT and F150A, we found that 2GBI needs to wait for the opening of an intracellular gate in order to gain access to the permeation pathway in the VSD, and that as long as the blocker is bound to its receptor, the gate cannot close. The increased affinity of the F150A channel for 2GBI and its faster kinetic of activation allowed us to investigate the recovery from block of dimeric and monomeric forms of Hv1. We found that when the open subunit of BO dimers closes, producing BC dimers, the release of 2GBI from the blocked subunit becomes substantially slower, as if the blocker was trapped inside the channel (hemichannel blocker trapping). We then analyzed the effect of 2GBI on the tail currents of F150A-WT linked dimers to confirm the delayed release of the trapped blocker.

Relative Stability of Hv1 Conformations and Blocker Trapping

The results of our simulations of Hv1 block support the idea that conformations in which the gates of the two subunits are out of sync (e.g., OC, and BC) are less stable than the conformations in which the gates are in sync (e.g., OO, CC, and BB). The energetic bias toward in-sync conformations could be due to mechanical stress between the two gates when one is open and the other is closed and can provide an explanation for the observed cooperativity between subunits during gating of Hv1 dimers (Fujiwara et al., 2012; Gonzalez et al., 2010; Musset et al., 2010; Tombola et al., 2010). The phenomenon of hemichannel blocker trapping can then be interpreted as a result of block-induced stabilization of BC dimers. In these dimers, the gate in the blocked subunit cannot close, forcing the two subunits to be out of sync. But, the blocked subunit can change conformation to increase the affinity for the blocker (~8-fold), and the stabilization of the channel associated with the tighter block can compensate for the destabilization caused by the stress between gates. This suggests that blockers capable of producing a strong stabilization of the hemichannel would be able to stay bound for a long time after channel activation, causing use-dependent cumulative block.

Relationship between F150 the Hv1 Selectivity Filter and the Gate

Unlike other ions, protons can move in aqueous solutions and within channel proteins via proton-hoping mechanism (Decoursey, 2003). The exact role played in proton-hoping by water inside the VSD (Ramsey et al., 2010; Wood et al., 2012) and by charged residues lining its pore is not well understood. But, recent studies have identified an aspartate in the middle of the S1 segment and the third S4 arginine (residues D112 and R211 in the human Hv1) as two key players in the ion selection mechanism (Berger and Isacoff, 2011; Musset et al., 2011). The region containing these two residues is likely to be the narrowest part of the permeation pathway.

Here, we find strong evidence that 2GBI binds in proximity of phenylalanine 150 in the S2 segment when blocking the proton pore. Different structural models of the Hv1 channel suggest that F150 is located just below D112 and R211 (or R3) in the core of the VSD (Ramsey et al., 2010; Wood et al., 2012), in other words, below the narrowest part of the permeation pathway. F150 corresponds to residue F233 in the Kv1.2-2.1 paddle chimera (Long et al., 2007). In the crystal structure of the potassium channel, F233 is located right on top of a cluster of tightly packed residues in which the fifth S4 charge (K5) interacts with two acidic residues in S2 and S3. Our findings suggest that in the Hv1 open conformation the corresponding cluster of tightly packed residues below the conserved phenylalanine is replaced by a vestibule large enough to accommodate the 2GBI blocker. This structural feature may be due to the lack of the fourth and fifth S4 charges in Hv1 and it is consistent with the idea that the narrowest part of the permeation pathway of the Hv1 channel—the selectivity filter—is located above F150, toward the extracellular side of the membrane.

In the pore domain, the activation gate and the selectivity filter are located on opposite sides of the membrane and so they are separated by a relatively large distance. In the VSD, selectivity filter and gate are likely to be much closer in space given the smaller size of the domain and the proximity of F150 to D112 and R211. In this context, the state dependence of 2GBI block could derive from the widening of the edges of the intracellular vestibule in the open state, which would allow the blocker to interact with a deeper binding site. Alternatively, it could derive from the formation of the intracellular binding site in the open state by the gating machinery.

Conclusions

The intracellular cavity of the pore domain can accommodate blockers of large size, including bulky quaternary ammonium ions. The intracellular vestibule of Hv1 on the other hand seems to fit guanidine derivatives like a tight glove. Even small differences in the structure of the blocker result in large variations in binding affinity (e.g., 2GBI versus GBOZ). Intracellular quaternary ammonium ions like TMA^+ and TEA^+ do not inhibit the Hv1 channel (Musset et al., 2011; Ramsey et al., 2006), either

because they cannot penetrate deep enough into the vestibule or because they lack the proper chemical properties for a tight binding. Exploring the specific interactions between guanidine derivatives and the intracellular vestibule of the Hv1 VSD will help develop inhibitors with higher affinity and selectivity for the channel.

Recently, Hv1 was found to be highly expressed in breast cancer cells, and its knockdown by RNA interference was shown to strongly reduce cell proliferation and invasiveness (Wang et al., 2011, 2012). Hv1 was also found to be involved in NOX-mediated neuronal death during cerebral ischemia, and mice lacking Hv1 activity were shown to be protected from brain damage after stroke (Wu et al., 2012). These findings highlight the importance of understanding how Hv1 works at the molecular level and how it can be modulated or blocked by small molecules like guanidine derivatives. The development of high-affinity inhibitors for Hv1 could lead to new chemotherapeutics and treatments for ischemic stroke.

The VSDs of voltage-gated sodium and potassium channels do not conduct ions under physiological conditions, but they can become ion permeable as a result of mutations in the voltage sensor (Sokolov et al., 2005; Starace and Bezanilla, 2004; Tombola et al., 2005). Ion/proton currents flowing through one of the VSDs of mutated Nav1.4 channels have been found to be the cause of some periodic paralyses (Sokolov et al., 2007; Struyk and Cannon, 2007). Mutations of voltage-gated ion channels associated with other genetic diseases have been proposed to result in ion conducting VSDs (Sokolov et al., 2007). Determining how the Hv1 channel is gated and how it interacts with small molecules could help design drugs able to block "leaky" VSDs.

EXPERIMENTAL PROCEDURES

Channel Expression in *Xenopus* Oocytes

Constructs containing the sequence of the human Hv1 channel were generated from cDNA kindly provided by David Clapham (Ramsey et al., 2006) and from IMAGE clone 5577070 (Open Biosystems). The cDNAs for Ci-VSP and Ci-VSOP were gifts from Yasushi Okamura (Murata et al., 2005; Sasaki et al., 2006). The cDNA for Eh-HVCN1 codon-optimized for expression in mammalian cells and *Xenopus* oocytes was kindly provided by Colin Brownlee and Glen Wheeler (Taylor et al., 2011). With the exception of Ci-VSOP, all the constructs were subcloned in the pGEMHE vector (Liman et al., 1992) by the SOEing technique (Horton et al., 1990). In the N_{VSP}-Hv1-C_{VSP} chimera, residues 1–96 and 228–273 of Hv1 were replaced by residues 1–113 and 240–576 of Ci-VSP, respectively. Single point mutations were introduced with standard PCR techniques. In the Hv1 linked dimers, the two consecutive subunits were connected by the sequence GGSGGSGGSGGSGGSGG (Tombola et al., 2008).

Plasmids were linearized with either NheI or SphI restriction enzymes (New England Biolabs) before in vitro transcription. RNA synthesis was carried out with a T7 mMessage mMachine transcription kit (Ambion). Ci-VSOP was in the pSD64TF expression vector (Krieg and Melton, 1984). The linearized plasmid was transcribed with SP6 RNA polymerase. cRNAs were injected in *Xenopus* oocytes (50 nl per cell, 0.3–1.5 μg/μl) 1–3 days before the electrophysiological measurements. Cells were kept at 18°C in ND96 medium containing 96 mM NaCl, 2 mM KCl, 1.8 mM $CaCl_2$, 1 mM $MgCl_2$, 10 mM HEPES, 5 mM pyruvate, 100 μg/ml gentamycin (pH 7.2).

Hv1 Inhibitors

All the compounds tested were at the highest purity commercially available. Guanidine hydrochloride was from MP Biomedicals. Aminoguanidine hydrochloride was from Acros Organics. 2-aminoimidazole sulfate, 2-aminopyrimidine, agmatine sulfate, 2-aminobenzimidazole, 2-guanidinobenzimidazole, 1,1-dimethylbiguanide hydrochloride, 2-guanidino-4-methylquinazoline hydrochloride, and N-(guanidino-imino-methyl)-N-phenylacetamide hydrochloride, were from Sigma-Aldrich. 1-(1,3-benzoxazol-2-yl)guanidine and 1-(1,3-benzothiazol-2-yl)guanidine were from both ChemDiv and Sigma-Aldrich. The compounds were directly dissolved in the recording solutions at the desired final concentrations or prepared as 100× stock solutions in the same medium. To keep GBOZ in solution at the highest concentrations tested on WT Hv1 channels, DMSO was added to a maximal ratio of 5% v/v for the 4 mM solution. We tested recording solutions with DMSO up to 10% v/v on inside-out patches containing Hv1 channels, and 5% was the maximal ratio that we were able to use without altering the measured proton currents or compromising the stability of the patch under perfusion.

We estimated the pK_a of the guanidinium group of the tested inhibitors using the pK_a calculation plugin of Marvin (http://www.ChemAxon.com). With the exception of 2-aminopyrimidine, the compounds were predicted to be primarily in the protonated and positively charged form at pH = 6.0. Compounds 7, 11, and 12 were also analyzed as free ligands in PROPKA3.1 (http://propka.ki.ku.dk) (Sondergaard et al., 2011). A charge of +1 was predicted for the three molecules under the pH conditions used for the measurements.

Patch-Clamp Measurements

Electrophysiological measurements on oocytes were performed in inside-out and outside-out patch configurations using an Axopatch 200B amplifier controlled by pClamp10 software through an Axon Digidata 1440A (Molecular Devices). Unless otherwise specified, the bath solution contained 100 mM 2-(N-morpholino)ethanesulphonic acid (MES), 30 mM tetraethylammonium (TEA) methanesulfonate, 5 mM TEA chloride, 5 mM ethyleneglycol-bis(2-aminoethyl)-N,N,N′,N′-tetra-acetic acid (EGTA), adjusted to pH 6.0 with TEA hydroxide. For recordings carried out in the absence of pH gradient (pH_i = pH_o = 6.0), the pipette solution had the same composition of the bath solution. Some of the measurements were performed in the presence of a pH gradient (pH_i = 6.0, pH_o = 7.5). In these cases the extracellular solution contained 100 mM 4-(2-hydroxyethyl)-1-piperazineethanesulfonic acid (HEPES), 40 mM TEA methanesulfonate, 5 mM TEA chloride, adjusted to pH 7.5 with TEA hydroxide. All measurements were performed at 22°C ± 2°C. Pipettes had 2–4 MΩ access resistance. Current traces were filtered at 1 kHz, sampled at 5 kHz and analyzed with Clampfit10.2 (Molecular Devices) and Origin8.1 (OriginLab).

Modeling of Channel Block

The process of channel block in dimeric and monomeric Hv1 was simulated with Berkeley Madonna 8.3 using the Runge-kutta 4 integration method (Macey et al., 2009). The model calculated the proton current in response to different voltage protocols in the absence and presence of 2GBI. The values of the rate constants used to generate the traces in Figures 6B–6D and S3 are reported in Figure S4. Dimeric channels were modeled by six distinct states (CC, OC, OO, BC, BO, BB), which took into account the fact that states OB, CB, and CO are equivalent to states BO, BC, and OC, respectively. Thus, at any point of time the total number of channels was represented by $N = N_{CC} + N_{OO} + N_{BB} + 2N_{OC} + 2N_{BO} + 2N_{BC}$.

SUPPLEMENTAL INFORMATION

Supplemental Information includes five figures, two tables, and Supplemental Experimental Procedures and can be found with this article online at http://dx.doi.org/10.1016/j.neuron.2012.11.013.

ACKNOWLEDGMENTS

We are grateful to D.E. Clapham for the cDNA of the h-Hv1 channel, Y. Okamura for the cDNAs of Ci-VSP and Ci-VSOP, and C. Brownlee and G. Wheeler for the cDNA of Eh-HVCN1. We thank M.L. Wood and D.J. Tobias for the Hv1-R1 and Hv1-R2 structural models superimposed in S1. This work was supported by the National Institute of Health (grant R01GM098973 to F.T.), the American Heart Association (WSA grant 09BGIA2160044 to F.T.), and the Helen Hay Whitney Foundation (postdoctoral fellowship to M.M.P.).

Accepted: November 9, 2012
Published: January 23, 2013

REFERENCES

Alabi, A.A., Bahamonde, M.I., Jung, H.J., Kim, J.I., and Swartz, K.J. (2007). Portability of paddle motif function and pharmacology in voltage sensors. Nature *450*, 370–375.

Armstrong, C.M. (1968). Induced inactivation of the potassium permeability of squid axon membranes. Nature *219*, 1262–1263.

Armstrong, C.M. (1971). Interaction of tetraethylammonium ion derivatives with the potassium channels of giant axons. J. Gen. Physiol. *58*, 413–437.

Armstrong, C.M., and Bezanilla, F. (1977). Inactivation of the sodium channel. II. Gating current experiments. J. Gen. Physiol. *70*, 567–590.

Berger, T.K., and Isacoff, E.Y. (2011). The pore of the voltage-gated proton channel. Neuron *72*, 991–1000.

Capasso, M., DeCoursey, T.E., and Dyer, M.J. (2011). pH regulation and beyond: unanticipated functions for the voltage-gated proton channel, HVCN1. Trends Cell Biol. *21*, 20–28.

Choi, K.L., Mossman, C., Aubé, J., and Yellen, G. (1993). The internal quaternary ammonium receptor site of Shaker potassium channels. Neuron *10*, 533–541.

Decoursey, T.E. (2003). Voltage-gated proton channels and other proton transfer pathways. Physiol. Rev. *83*, 1067.

DeCoursey, T.E., and Cherny, V.V. (2007). Pharmacology of voltage-gated proton channels. Curr. Pharm. Des. *13*, 2400–2420.

Demo, S.D., and Yellen, G. (1991). The inactivation gate of the Shaker K+ channel behaves like an open-channel blocker. Neuron *7*, 743–753.

Fujiwara, Y., Kurokawa, T., Takeshita, K., Kobayashi, M., Okochi, Y., Nakagawa, A., and Okamura, Y. (2012). The cytoplasmic coiled-coil mediates cooperative gating temperature sensitivity in the voltage-gated H(+) channel Hv1. Nat. Commun. *3*, 816.

Gonzalez, C., Koch, H.P., Drum, B.M., and Larsson, H.P. (2010). Strong cooperativity between subunits in voltage-gated proton channels. Nat. Struct. Mol. Biol. *17*, 51–56.

Hille, B. (2001). Ion Channels of Excitable Membranes, Third Edition (Sunderland: Sinauer Associates Inc.).

Holmgren, M., Smith, P.L., and Yellen, G. (1997). Trapping of organic blockers by closing of voltage-dependent K+ channels: evidence for a trap door mechanism of activation gating. J. Gen. Physiol. *109*, 527–535.

Horton, R.M., Cai, Z.L., Ho, S.N., and Pease, L.R. (1990). Gene splicing by overlap extension: tailor-made genes using the polymerase chain reaction. Biotechniques *8*, 528–535.

Kalia, J., and Swartz, K.J. (2011). Elucidating the molecular basis of action of a classic drug: guanidine compounds as inhibitors of voltage-gated potassium channels. Mol. Pharmacol. *80*, 1085–1095.

Koch, H.P., Kurokawa, T., Okochi, Y., Sasaki, M., Okamura, Y., and Larsson, H.P. (2008). Multimeric nature of voltage-gated proton channels. Proc. Natl. Acad. Sci. USA *105*, 9111–9116.

Krieg, P.A., and Melton, D.A. (1984). Functional messenger RNAs are produced by SP6 in vitro transcription of cloned cDNAs. Nucleic Acids Res. *12*, 7057–7070.

Lacroix, J.J., and Bezanilla, F. (2011). Control of a final gating charge transition by a hydrophobic residue in the S2 segment of a K+ channel voltage sensor. Proc. Natl. Acad. Sci. USA *108*, 6444–6449.

Lee, S.Y., Letts, J.A., and Mackinnon, R. (2008). Dimeric subunit stoichiometry of the human voltage-dependent proton channel Hv1. Proc. Natl. Acad. Sci. USA *105*, 7692–7695.

Lee, S.Y., Letts, J.A., and MacKinnon, R. (2009). Functional reconstitution of purified human Hv1 H+ channels. J. Mol. Biol. *387*, 1055–1060.

Li, S.J., Zhao, Q., Zhou, Q., Unno, H., Zhai, Y., and Sun, F. (2010). The role and structure of the carboxyl-terminal domain of the human voltage-gated proton channel Hv1. J. Biol. Chem. *285*, 12047–12054.

Liman, E.R., Tytgat, J., and Hess, P. (1992). Subunit stoichiometry of a mammalian K+ channel determined by construction of multimeric cDNAs. Neuron *9*, 861–871.

Long, S.B., Tao, X., Campbell, E.B., and MacKinnon, R. (2007). Atomic structure of a voltage-dependent K+ channel in a lipid membrane-like environment. Nature *450*, 376–382.

Macey, R., Oster, G., and Zahnley, T. (2009). Berkeley Madonna User's Guide Version 8.0, available from: http://wwwberkeleymadonna.com

Murata, Y., Iwasaki, H., Sasaki, M., Inaba, K., and Okamura, Y. (2005). Phosphoinositide phosphatase activity coupled to an intrinsic voltage sensor. Nature *435*, 1239–1243.

Musset, B., Cherny, V.V., Morgan, D., Okamura, Y., Ramsey, I.S., Clapham, D.E., and DeCoursey, T.E. (2008). Detailed comparison of expressed and native voltage-gated proton channel currents. J. Physiol. *586*, 2477–2486.

Musset, B., Smith, S.M., Rajan, S., Cherny, V.V., Sujai, S., Morgan, D., and DeCoursey, T.E. (2010). Zinc inhibition of monomeric and dimeric proton channels suggests cooperative gating. J. Physiol. *588*, 1435–1449.

Musset, B., Smith, S.M., Rajan, S., Morgan, D., Cherny, V.V., and Decoursey, T.E. (2011). Aspartate 112 is the selectivity filter of the human voltage-gated proton channel. Nature *480*, 273–277.

Narahashi, T., Yamada, M., and Frazier, D.T. (1969). Cationic forms of local anaesthetics block action potentials from inside the nerve membrane. Nature *223*, 748–749.

Okamura, Y. (2007). Biodiversity of voltage sensor domain proteins. Pflugers Arch. *454*, 361–371.

Ramsey, I.S., Moran, M.M., Chong, J.A., and Clapham, D.E. (2006). A voltage-gated proton-selective channel lacking the pore domain. Nature *440*, 1213–1216.

Ramsey, I.S., Mokrab, Y., Carvacho, I., Sands, Z.A., Sansom, M.S., and Clapham, D.E. (2010). An aqueous H+ permeation pathway in the voltage-gated proton channel Hv1. Nat. Struct. Mol. Biol. *17*, 869–875.

Sasaki, M., Takagi, M., and Okamura, Y. (2006). A voltage sensor-domain protein is a voltage-gated proton channel. Science *312*, 589–592.

Sokolov, S., Scheuer, T., and Catterall, W.A. (2005). Ion permeation through a voltage- sensitive gating pore in brain sodium channels having voltage sensor mutations. Neuron *47*, 183–189.

Sokolov, S., Scheuer, T., and Catterall, W.A. (2007). Gating pore current in an inherited ion channelopathy. Nature *446*, 76–78.

Sokolov, S., Scheuer, T., and Catterall, W.A. (2010). Ion permeation and block of the gating pore in the voltage sensor of NaV1.4 channels with hypokalemic periodic paralysis mutations. J. Gen. Physiol. *136*, 225–236.

Sondergaard, C.R., Olsson, M.H.M., Rostkowski, M., and Jensen, J.H. (2011). Improved Treatment of Ligands and Coupling Effects in Empirical Calculation and Rationalization of pK(a) Values. J. Chem. Theory Comput. *7*, 2284–2295.

Starace, D.M., and Bezanilla, F. (2004). A proton pore in a potassium channel voltage sensor reveals a focused electric field. Nature *427*, 548–553.

Struyk, A.F., and Cannon, S.C. (2007). A Na+ channel mutation linked to hypokalemic periodic paralysis exposes a proton-selective gating pore. J. Gen. Physiol. *130*, 11–20.

Tao, X., Lee, A., Limapichat, W., Dougherty, D.A., and MacKinnon, R. (2010). A gating charge transfer center in voltage sensors. Science *328*, 67–73.

Taylor, A.R., Chrachri, A., Wheeler, G., Goddard, H., and Brownlee, C. (2011). A voltage-gated H+ channel underlying pH homeostasis in calcifying coccolithophores. PLoS Biol. *9*, e1001085.

Tombola, F., Pathak, M.M., and Isacoff, E.Y. (2005). Voltage-sensing arginines in a potassium channel permeate and occlude cation-selective pores. Neuron *45*, 379–388.

Tombola, F., Pathak, M.M., Gorostiza, P., and Isacoff, E.Y. (2007). The twisted ion-permeation pathway of a resting voltage-sensing domain. Nature *445*, 546–549.

Tombola, F., Ulbrich, M.H., and Isacoff, E.Y. (2008). The voltage-gated proton channel Hv1 has two pores, each controlled by one voltage sensor. Neuron *58*, 546–556.

Tombola, F., Ulbrich, M.H., Kohout, S.C., and Isacoff, E.Y. (2010). The opening of the two pores of the Hv1 voltage-gated proton channel is tuned by cooperativity. Nat. Struct. Mol. Biol. *17*, 44–50.

Wang, Y., Li, S.J., Pan, J., Che, Y., Yin, J., and Zhao, Q. (2011). Specific expression of the human voltage-gated proton channel Hv1 in highly metastatic breast cancer cells, promotes tumor progression and metastasis. Biochem. Biophys. Res. Commun. *412*, 353–359.

Wang, Y., Li, S.J., Wu, X., Che, Y., and Li, Q. (2012). Clinicopathological and biological significance of human voltage-gated proton channel Hv1 protein overexpression in breast cancer. J. Biol. Chem. *287*, 13877–13888.

Wood, M.L., Schow, E.V., Freites, J.A., White, S.H., Tombola, F., and Tobias, D.J. (2012). Water wires in atomistic models of the Hv1 proton channel. Biochim. Biophys. Acta *1818*, 286–293.

Woodhull, A.M. (1973). Ionic blockage of sodium channels in nerve. J. Gen. Physiol. *61*, 687–708.

Wu, L.J., Wu, G., Akhavan Sharif, M.R., Baker, A., Jia, Y., Fahey, F.H., Luo, H.R., Feener, E.P., and Clapham, D.E. (2012). The voltage-gated proton channel Hv1 enhances brain damage from ischemic stroke. Nat. Neurosci. *15*, 565–573.

Yeh, J.Z., and Armstrong, C.M. (1978). Immobilisation of gating charge by a substance that simulates inactivation. Nature *273*, 387–389.

Yu, F.H., and Catterall, W.A. (2004). The VGL-chanome: a protein superfamily specialized for electrical signaling and ionic homeostasis. Sci. STKE *2004*, re15.

Zagotta, W.N., Hoshi, T., and Aldrich, R.W. (1990). Restoration of inactivation in mutants of Shaker potassium channels by a peptide derived from ShB. Science *250*, 568–571.